High-speed modified uni-traveling-carrier photodiode with a new absorber design

Liqing Guo (郭丽庆)*, **Yongqing Huang (黄永清)**, **Xiaofeng Duan (段晓峰)**, **Xiaomin Ren (任晓敏)**, **Qi Wang (王 琦)**, and **Xia Zhang (张 霞)**

State Key Lab of Information Photonics and Optical Communications, Institute of Information Photonics and Optical Communications, Beijing University of Posts and Telecommunications, Beijing 100876, China

**Corresponding author: glqbupt@163.com*

Received August 9, 2011; accepted September 29, 2011; posted online April 18, 2012

The Gaussian doping is used to optimize the performance of InP/InGaAs uni-traveling-carrier photodiode (UTC-PD) in this letter. The UTC-PD structure is modeled with drift-diffusion approach and the comparisons of the characteristics for four UTC-PDs with different doping schemes in absorption layer are made. According to the comparison, one optimized UTC-PD where the InP collection layer is partly replaced by a depleted InGaAs using Gaussian doping on top of lightly constant background doping in the absorption layer is presented, with f_{3dB} of 79 GHz, which is more than 1.9 times higher than that with the constant doping in the absorption layer.

OCIS codes: 230.0230, 230.0040, 230.5170.

doi: 10.3788/COL201210.S12301.

Progress in fiber-optic communication system demands innovative improvements in device performances. As an essential optical-to-electrical (O/E) interface component in the system, photo detector (PD) is one of the crucial elements that dictate the overall system performance. In general, bandwidth and quantum efficiency are important figures of merit for high-speed PDs, though constraints exist due to the tradeoff between these characteristics[1]. With the advent of optical amplifier, the high-output capability of a PD has also become very important. The uni-traveling-carrier photodiode (UTC-PD) with a high-saturation output power and a high speed response simultaneously has been developed by NTT System Electrons Laboratories , which uses the electrons as the only active carrier traveling through the junction depletion later[2,3].

To date, many UTC-PDs have been fabricated and a great progress in device design and fabrication have been made. According to difference on the methods of the light coupling, there are back-illuminated UTC-PD[1−5], edge-coupled waveguide UTC-PD (UTC-WGPD)[6], and UTC-PD with an integrated total-reflection mirror[7]. Excellent performance, including a 3-dB-down-bandwidth of 310 GHz and an output power of over 20 mW at 100 GHz[8], has already been demonstrated. Recently, a linear cascade near-ballistic uni-traveling-carrier photodiodes with saturation-current-bandwidth product (SCBP) 6 825 mA-GHz at 91 GHz under the 50 Ω load resistance has been reported[9−11].

In this letter, we introduce an electric field by using Gaussian doping in the absorption region to optimize the performance of UTC-PD, and simulate the characteristics of four UTC-PDs with four different doping schemes in the absorption layer with a numerical device simulator ATLAS. The comparisons of the characteristics for the devices with different doping scheme are given. And according to the comparisons, we present an optimized device that can obtain high speed without decreasing the responsivity.

The energy band diagram of UTC-PD is shown in the Fig. 1. The most important feature in the structure is the separation of absorption and collection region. The structure includes a p-type InGaAs light absorption region and an InP wide-gap collection region. The electron-hole pairs are generated when the light is absorbed in p-doped InGaAs absorption region. The minority electrons generated in absorption region diffuse towards anode side, and are blocked by the diffusion barrier layer. The electrons diffuse towards the InP collection region and are swept across to the subcollection by the large depletion field. On the other hand, holes are majority carriers in the absorption region, and the hole energy relaxation time is very small so that the response times of the photogenerated holes are ignored. Therefore, the photoresponse of UTC-PD is primarily determined by the electron transport[12,13].

For the normal UTC-PDs, the electric field in the

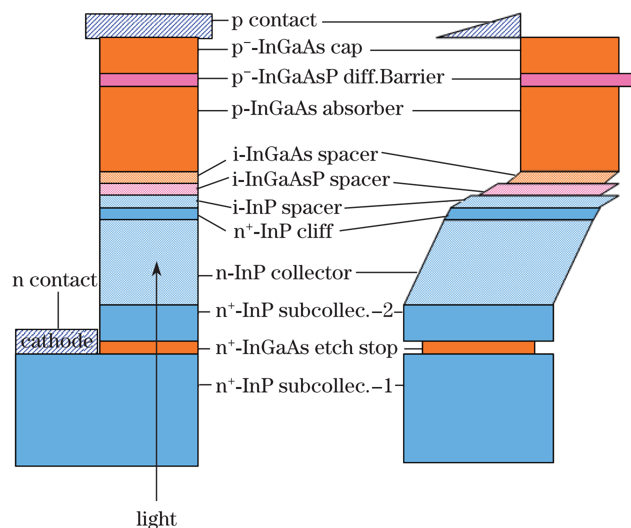

Fig. 1. Energy band diagram of UTC-PD.

 © 2012 Chinese Optics Letters

absorption is very small since it is highly doped, which results in only diffusion component in electron current. So we introduce an electric field in the absorption region to optimize the performance. It is reported that even slow gradient of acceptors concentration create internal built-in electric field[14]. The UTC-PD with variable doping in the absorption region have already been investigated. In Refs. [4,5], the author used step-graded doping and linear doping respectively. From the references, we know that the optimized performances are very impressive. So, we try to use Gaussian doping in absorption region to optimize the device.

In this letter, the drift-diffuse model is used to describe the carrier transport. The ATLAS software is used to solve the required equations to predict the electrical characteristics. In the simulation, the bottom illumination is at 1.55-μm-wavelength, 2-V reverse bias, and 14-μm^2 device area. Concentration dependent mobility model namely ANALYTIC and CONMOB, field dependent mobility model namely FLDMOB, and recombination model namely SRH and CONSRH, are used in the simulation[15]. The epitaxial layer structure for InP/InGaAs UTC-PD is showed in Table 1. The parameters used in the simulation are obtained from the reference[12].

According to the Refs. [14,16], the non-uniform doping results in a built-in electric field, and the electric field can be expressed as

$$E_x = \pm\left(\frac{k_\text{B}T}{q}\right)\frac{1}{N(x)}\frac{\text{d}N(x)}{\text{d}x}, \tag{1}$$

where k_B is Boltzmann constant, T is the temperature, q is electron charge, and $N(x)$ is the doping concentration.

In this letter, $N(x)$ is the Gaussian distribution, and is given as

$$N(x) = \text{conc}\cdot\exp\left[-\frac{(x-\text{peak})^2}{\text{char}^2}\right], \tag{2}$$

where conc is defined as the peak concentration of the Gaussian distribution, char/$\sqrt{2}$ is the standard deviation, and peak specifies the depth location of the peak doping in a Gaussian profile[15]. For the absorption of UTC-PD, the highly doping is required. To avoid the absorption layer doping falling to a very low level at the collection end of the absorption layer, a constant p doping is used as a background doping.

Table 1. Epitaxial Layer Structure for UTC-PD Used in Simulation

Layer	Thickness (nm)	Doping (cm^{-3})	Band-Gap (eV)
p^--InGaAs Cap	50	3×10^{19}	0.734
p^--InGaAsP Diff.Barrier	20	2×10^{19}	0.85
p-InGaAs Absorber	220	Gaussian Doping	0.734
i-InGaAs Spacer	8	1×10^{15}	1.0
i-InGaAsP Spacer	16	1×10^{15}	1.35
i-InP Spacer	6	1×10^{15}	1.35
n^--InP Cliff	7	1×10^{15}	1.35
n-InP Collector	267	1×10^{15}	1.35
n^--InP Suboollec.-2	50	5×10^{15}	1.35
n^--InGaAs Etch Stop	10	1.5×10^{19}	0.734
n^--InP Suboollec.-1	500	1.5×10^{19}	1.35

We consider a p-type semiconductor doped with acceptor impurity, and the impurity distribution is Gaussian doping with the location of peak doping at 1.08 μm on the top of constant background doping. Figure 2 shows the Gaussian doping schemes with different parameters and the built-in electric field result from Gaussian doping. In Fig. 2, the base parameter is defined as the background doping. We can find that the doping concentration become flatter with the char parameter increasing, resulting in that the built-in electric field become flatter and the peak of the electric field move far away from the location of peak doping, correspondingly. In addition, the built-in electric field increases with the background doping decreasing and the peak doping increasing. We also find that all the peaks of the built-in electric field are bigger than 3 000 V/cm.

According to the discussion above, the Gaussian doping with suitable parameters in semiconductor can introduce a build-in electric field that have great influence on the characteristic of the semiconductor device ultimately. It is well known that the mobility depends on the doping level and the local electric field. The mobility of electrons and holes in InGaAs has been studied theoretically and experimentally[12]. For the Gaussian doping, conc, char, and background doping should be better designed to obtain suitable build-in electric field for making the total response current in the absorption layer as an superposition of the diffusion current and the drift current.

We designed and simulated four UTC-PDs with four different doping schemes in the absorption layer. Table 2 gives the parameters for these four doping schemes.

Figure 3(a) shows the four different doping schemes used in the absorption layer of UTC-PD. Figures 3(b) and (c) show the energy band diagram of InGaAs/InP UTC-PD with four doping schemes in the absorption layer. For the constant doping, the energy band is flat whereas with Gaussian doping schemes. There is a slope with different degree in the energy band. The slope in

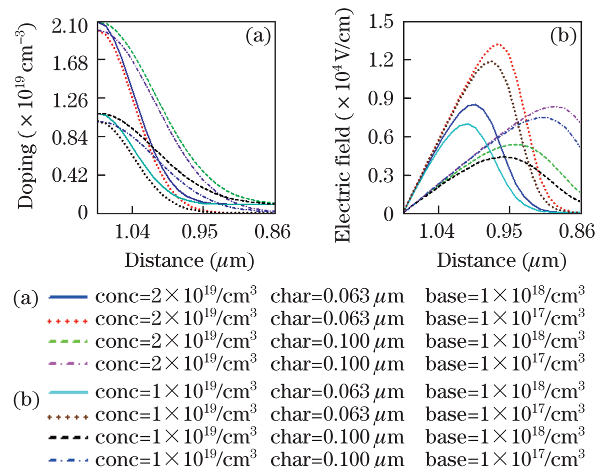

Fig. 2. (a) Gaussian doping schemes with different parameters and (b) the built-in electric field result from Gaussian doping.

Table 2. Parameters for Four Different Doping Schemes

Type	Distribution Doping	conc (cm^{-3})	base (cm^{-3})	peak (μm)	char (μm)
I	Constant	1×10^{18}			
II	Gaussian -Constant	2×10^{19}	1×10^{17}	1.08	0.063
III	Gaussian -Constant	2×10^{19}	1×10^{18}	1.08	0.063
IV	Gaussian -Constant	2×10^{19}	1×10^{18}	1.08	0.1

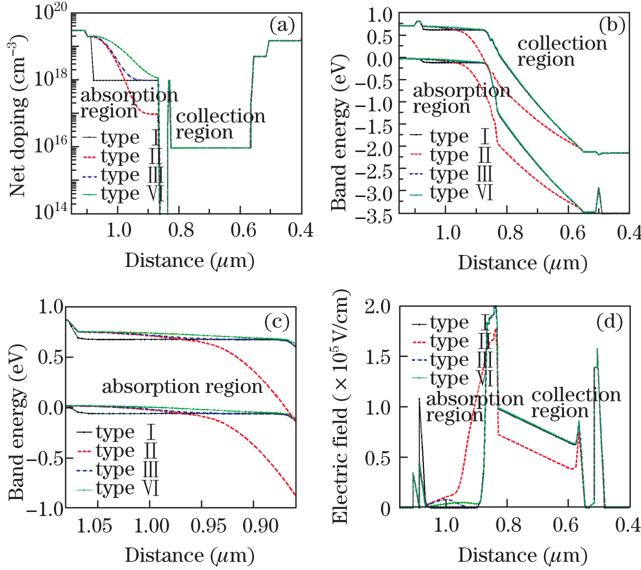

Fig. 3. Comparison of the internal device parameter distributions of InGaAs/InP UTC-PDs: (a) net doping scheme, (b) energy band diagram, (c) enlarged view of the energy band in the absorption layer, and (d) electric field profile for a reverse bias of 2 V, DC optical intensity of 2×10^5 W/cm^2.

the conduction band encourages the electrons to drift towards the collection layer end and holes towards the blocking layer end of the absorption layer. It is remarkable that the type II has a large slope in the energy band after the intersection of the lines for types I and II near the center of the absorption region, and has a downward displacement in collection layer compared with other three types.

The electric field profiles across the device with different doping schemes are shown in the Fig. 3(d). The electric field at each heterojunction interface is very large as expected due to the conduction band discontinuity. The electric field profile in the absorption for the type I is almost zero due to the constant doping, whereas that for other three types is significant, especially the type II with its electric field approximately 1.5×10^5 V/cm at the collection layer end of the absorption layer. In the collection layer, the electric field is also large and that for the type II is lower that others.

Figure 4 shows the responsivity and small signal AC characteristics of the device. The responsivity with doping scheme types II and III indicates a slight improvement, while that with doping scheme type IV indicates a reduction. In fact, the effect of varying the doping of the absorption is to modify the diffusion length, which is given by $L_e = \sqrt{D_e\tau_e} = \sqrt{\frac{k_BT}{q}\mu_e(N)\tau_e(N)}$, where $\mu_e(N)$ and $\tau_e(N)$, are electron mobility and minority carrier lifetimes, which depend on the doping[12]. On the other hand, μ_e is also the function of the electric field. Thus, when L_e depending on the doping and electric field becomes comparable to the absorption layer thickness, the collection of the photogenerated electrons becomes less efficient and the responsivity drops. The frequency response is showed in Fig. 4(b). For the device with constant doping scheme, the 3-dB-down-frequency is 41.79 GHz, whereas for the device with doping scheme type II the 3-dB-down-frequency is 79.22 GHz, which is more than 1.9 times higher than that with the constant doping. And for the devices with doping scheme types III and IV also have an enhancement in 3-dB-down-frequency but not larger than that for type II. The build-in electric field resulting from the Gaussian doping should be the main reason for the enhancement in frequency response.

To better understand the relationship between the 3-dB-down-frequency and the Gaussian doping, another five structures with the Gaussian doping schemes listing at the Fig. 2 are simulated further, and the results are marked on Fig. 2(b), and redrawn in Fig. 5. For

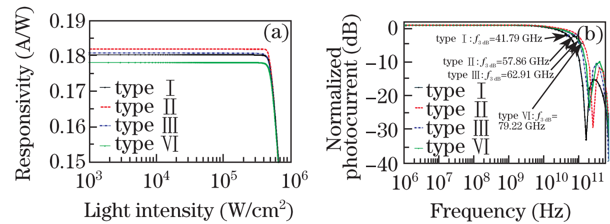

Fig. 4. Comparison of characteristics of InGaAs/InP UTC-PD: (a) the responsivity versus light intensity at 2-V-bias, (b) small-signal photocurrent response versus frequency at 2-V-bias, DC optical intensity of 2×10^5 W/cm^2 and AC optical intensity of 1×10^3 W/cm^2.

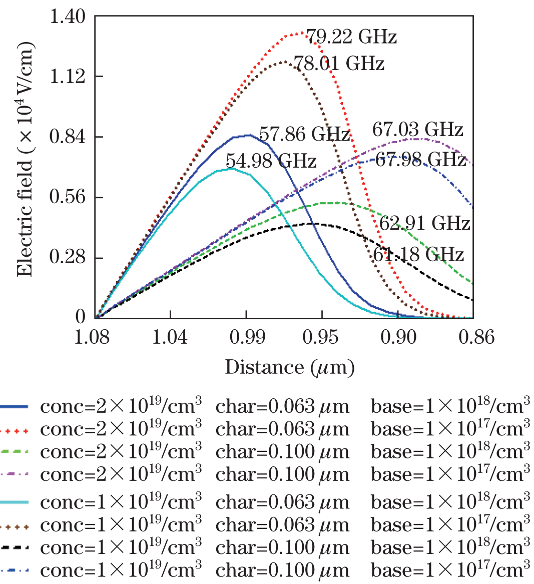

Fig. 5. 3-dB-down-frequency with different Gaussian doping schemes at 2-V-bias, DC optical intensity of 2×10^5 W/cm^2 and AC optical intensity of 1×10^3 W/cm^2.

the highly background doping ($1 \times 10^{18}/\text{cm}^3$), the bigger char parameter is the higher bandwidth is, and the higher peak doping concentration is the higher bandwidth is. Whereas, for the lightly background doping ($1\times10^{17}/\text{cm}^3$), it is the char parameter bigger the bandwidth smaller, and with the peak doping concentration increasing, the variety of bandwidth is not obvious. This is because of that the Gaussian doping with lightly background doping and small char parameter (0.63 μm) divides the absorption layer into a heavy gradated doping region and a lightly doping depleted collecting region, helping the carriers transient to the InP collection rapidly.

According to the discussion above, we found that the device with doping scheme type II had higher responsivity and speed. This is not only explained as introducing a electric field, but also as dividing the absorption layer into a heavy doping region and a lightly doping region, which also act as a depleted collection layer just like InP collection layer. In other word, the device with where the collection layer is partly replaced by a depleted InGaAs can obtain high speed without decreasing the responsivity.

Figure 6 shows the 3-dB-down-bandwidth versus DC optical intensity of the device with doping scheme type II. It is observed that the 3-dB-down-bandwidth remains constant (~79 GHz) at small intensity ($\leqslant 2\times10^5$ W/cm^2) and drops down sharply at higher intensity levels ($> 4 \times 10^5$ W/cm^2) due to the onset of high optical injection and its associated space charge effects.

In conclusion, the Gaussian doping in semiconductor is discussed and used in the absorption layer of UTC-PD to optimize the performance. In this letter, the drift-diffusion approach is utilized to analyze the characteristics of device, and the characteristics of four UTC-PDs with four different doping schemes in the absorption layer are modeled and simulated by ATLAS. From the comparison, we can obtain an optimized UTC-PD with Gaussian doping on the top of lightly constant background doping in the absorption layer has a –3-dB-bandwidth of 79 GHz at small intensity, and a responsivity of 0.182 A/W.

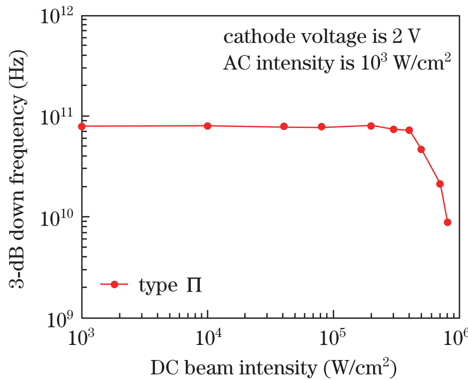

Fig. 6. 3-dB-down-frequency versus DC optical intensity at 2-V bias of the device with doping scheme type II.

This work was supported by the National 973 Program of China (No. 2010CB327600), the National Natural Science Foundation of China (No. 61020106007), the Fundamental Research Funds for the Central University (No. BUPT2011RC0403), the National 863 Program of China (No. 2007AA03Z418), the 111 Project of China (No. B07005), and the Program for Changjiang Scholars and Innovative Research Team in University (No. IRT0609), MOE, China.

References

1. H. Ito, S. Kodama, Y. Muramoto, T. Furuta, T. Nagatsuma, and T. Ishibashi, IEEE J. Sel. Top. Quantum Electron. **10,** 709 (2004).
2. T. Ishibashi, S. Kodama, N. Shimizu, and T. Furuta, Jpn. J. Appl. Phys. **36,** 6263 (1997).
3. T. Ishibashi, T. Furuta, H. Fushimi, and S. Kodama, IEICE Trans. Electron. E83-C. **6,** 938 (2000).
4. N. Shimizu, N. Watanabe, T. Furuta, and T. Ishibashi, in *Proceedings of Device Research Conference Digest* 164 (2001).
5. G. Li, Y. Zhang, X. Li, and L. Tian, J. Semi. **31,** 38 (2010).
6. Y. Muramoto, K. Kato, M. Mitsuhara, O. Nakajima, Y. Matsuoka, N. Shimizu, and T. Ishibashi, Electron. Lett. **34,** 122 (1998).
7. H. Ito, T. Furuta, S. Kodama, and T. Ishibashi, IEEE J. Lightwave Technol. **18,** 384 (2000).
8. A. Wakatsuki, T. Furuta, Y. Muramoto, and T. Ishibashi, in *Proceedings of Optical Fiber Communication Conference, OSA Technical Digest (CD)* OMK1 (2009).
9. J. Shi, F. Kuo, and M. Chou, in *Proceedings of National Fiber Optic Engineers Conference, OSA Technical Digest (CD)* PDPA6 (2010).
10. J. Shi, F. Kuo, C. Chang, C. Chang, C. Liu, and J. Chyi, IEEE J. Quantum Electron. **46,** 80 (2010).
11. J. Shi, Y. Wu, C. Wu, P. Chiu, and C. Hong, IEEE Photon. Technol. Lett. **17,** 1929 (2005).
12. S. Srivastava, "Simulation Study of InP-Based Uni-Traveling Carrier Photodiode", PhD. Thesis (Pune University, 2003).
13. S. Xie, L. Liu, W. Kang, R. Song, L. Mao, and S. Zhang, Chin. Sci. Bull. **54,** 3691 (2009).
14. F. V. Gasparyan, V. M. Aroutiounian, Y. A. Abrahamian, and A. I. Vahanian, Sens. Actua. A Phy. **113,** 370 (2004).
15. S. Clara, *ATLAS Users Manual* (Silvaco International, 2008).
16. D. A. Neamen, *Semiconductor Physics and Devices Basic Principles* (McGraw-Hill, New York, 2003).